DRAGON Stable Beam Optics Commissioning: The Wobbler Study

Dustin Lang

April 20, 2002

1 Introduction

During the week of January 14 through 18, 2002, a stable beam commissioning study of the DRAGON optics was performed. This report presents a summary and the results of that study.

A beam of Neon-20 at energies of 194, 200, and 206 keV/u was employed. Beam current was approximately 5 nA, and charge state 4+ was used. In the week prior to the study the *wobbler* magnet (a 4-inch steering magnet) was installed at the gas target. No gas was present during the study.

The wobbler magnet allows the beam to be steered independently in the two transverse directions (x and y). "Wobbling" the beam allows controlled measurement of the response of the DRAGON optics to ions leaving the gas cell with non-zero transverse velocity. Since recoils leave the gas cell with a cone of transverse velocities, it is important that this aspect of the DRAGON's performance be understood.

In addition to transverse velocities, recoils have a range of velocities in the forward direction. This corresponds to a differences in energy. In order to study the behaviour of such ions, the beam energy was varied by 6 keV/u from the central value of 200 keV/u. The DRAGON was *not* retuned for these energies so that the effects of energy difference could be studied.

The beam profiles at the charge, mass, and final slits were measured using the slits and Faraday cups. Therefore, this study investigated the effects of three parameters (transverse velocities and energy difference) on the position of the beam in the transverse plane.

2 Experiment Setup and Data Collection

2.1 Terminology

This report will adopt the coordinate system used by GIOSP. The optic axis of the DRAGON defines the z direction, with downstream being the positive direction. Looking downstream, the positive x direction is to the left, while the positive y direction is up. An ion's transverse velocity is described by a and b, the angles between the ion's x and y velocity components (respectively) and the z velocity component.

GIOSP considers the position and velocity of an ion at any point in the DRAGON to be functions of the initial position, velocity, energy, and mass.

The DRAGON is tuned so that an ion with a specific set of initial conditions follows the z-axis through the system. Such an ion is called a reference ion. In order to characterise the behaviour of ions with slightly different initial conditions, a Taylor expansion is taken about these reference conditions. This expansion can be expressed compactly in matrix form:

$$\begin{bmatrix} x \\ y \\ a \\ b \end{bmatrix} = \begin{bmatrix} (x|a) & (x|b) & (x|d) & (x|g) \\ (y|a) & (y|b) & (y|d) & (y|g) \\ (a|a) & (a|b) & (a|d) & (a|g) \\ (b|a) & (b|b) & (b|d) & (b|g) \end{bmatrix} \begin{bmatrix} a \\ b \\ d \\ g \end{bmatrix}$$
$$+ \begin{bmatrix} (x|aa) & (x|bb) & (x|ab) & (x|da) & (x|db) \\ (y|aa) & (y|bb) & (y|ab) & (y|da) & (y|db) \\ (a|aa) & (a|bb) & (a|ab) & (a|da) & (a|db) \\ (b|aa) & (b|bb) & (b|ab) & (b|da) & (b|db) \end{bmatrix} \begin{bmatrix} a^2 \\ b^2 \\ ab \\ da \\ db \end{bmatrix}$$
$$+ \cdots$$

where:

a : angle between ion's x-component and z-component of velocity.
b : angle between ion's y-component and z-component of velocity.
g : ion's fractional mass difference from the reference ion.
d : ion's fractional energy difference from the reference ion.

In this study only the a, b, and d parameters and their second-order combinations were varied, and the x and y results were measured. We therefore measured the first two rows of this matrix expression (except for the g elements).

2.2 Wobbler Collimator

The wobbler magnet incorporates a square 3 mm aperture whose position can be adjusted. It was thought that it would be necessary to adjust the position of the aperture with wobble angle in order to allow full beam transmission. However, measurements showed that this was not the case and the aperture was therefore kept stationary during this study.[1]

[1] DRAGON Logbook #6, pg. 8-12.

2.3 Hardware

The scanning technique used in this run employed the Faraday cups and slits at the charge, mass, and final foci. The slit width was set to one or two millimeters and stepped in one or two millimeter steps across the beam profile. At each step the beam current striking the Faraday cup was measured. Scanning the x and y slits allowed the horizontal and vertical beam profiles to be measured separately.

A slight complication arose due to the Faraday cup current measurement electronics and EPICS software. While the hardware allows a sampling rate of approximately 10 Hz, the EPICS software performs averaging of the measurements.[2] This has the same effect as introducing a smoothing resistor-capacitor circuit with time constant $\tau \simeq 2s$ at the input to the analog-to-digital converter. This meant that rather than scanning the slits quickly it was necessary to pause for several seconds before taking each Faraday cup current reading.

2.4 Software

The scanning operation involves moving the slits, waiting, measuring the Faraday cup current, and repeating. Since each scan required at least ten points and there were several hundred scans to be performed, automation of the process was necessary. As no existing software was available, the program `slitscan` was written to perform the scans.

The `slitscan` program uses the EPICS Channel Access library. This library allows EPICS devices to be monitored and controlled through a flexible `C` language interface. The Channel Access library is also used by the standard graphical EPICS software `DM`.

The EPICS system uses a host-based security policy to determine whether a request to read or set an EPICS device will be granted or denied. For ease of administration, access to EPICS devices at TRIUMF is centralised in several Sun servers maintained by the Controls group. Since `slitscan` was developed to run on the DRAGON computers, it was necessary to request access to the EPICS system from the Controls group. The machine `isdaq04` was granted full access to the DRAGON EPICS devices.

The `slitscan` configuration window (see Figure 2.4) allows the user to select the slits to be scanned, the limits of the scan, the step size, and so on.

[2] Daryl Bishop, personal communication 11 Apr 2002.

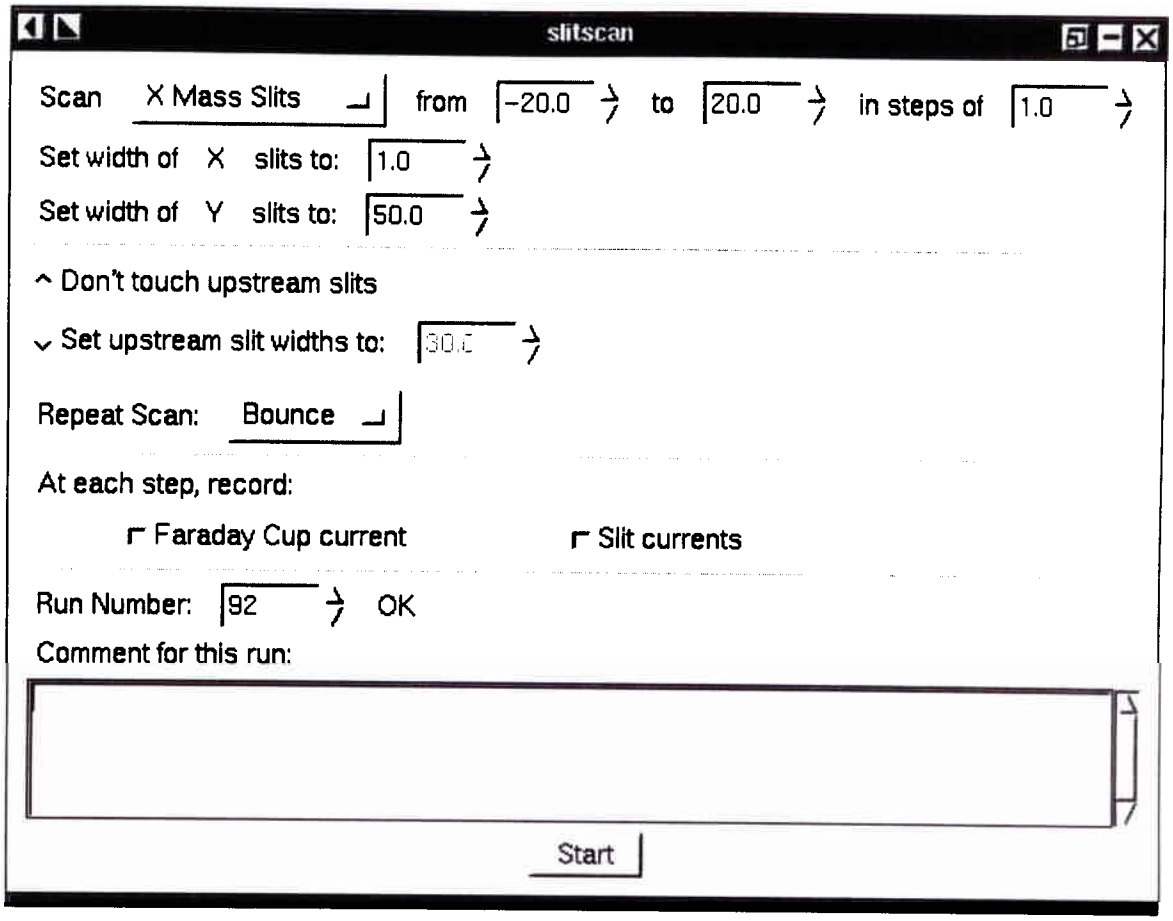

Figure 1: First **slitscan** window

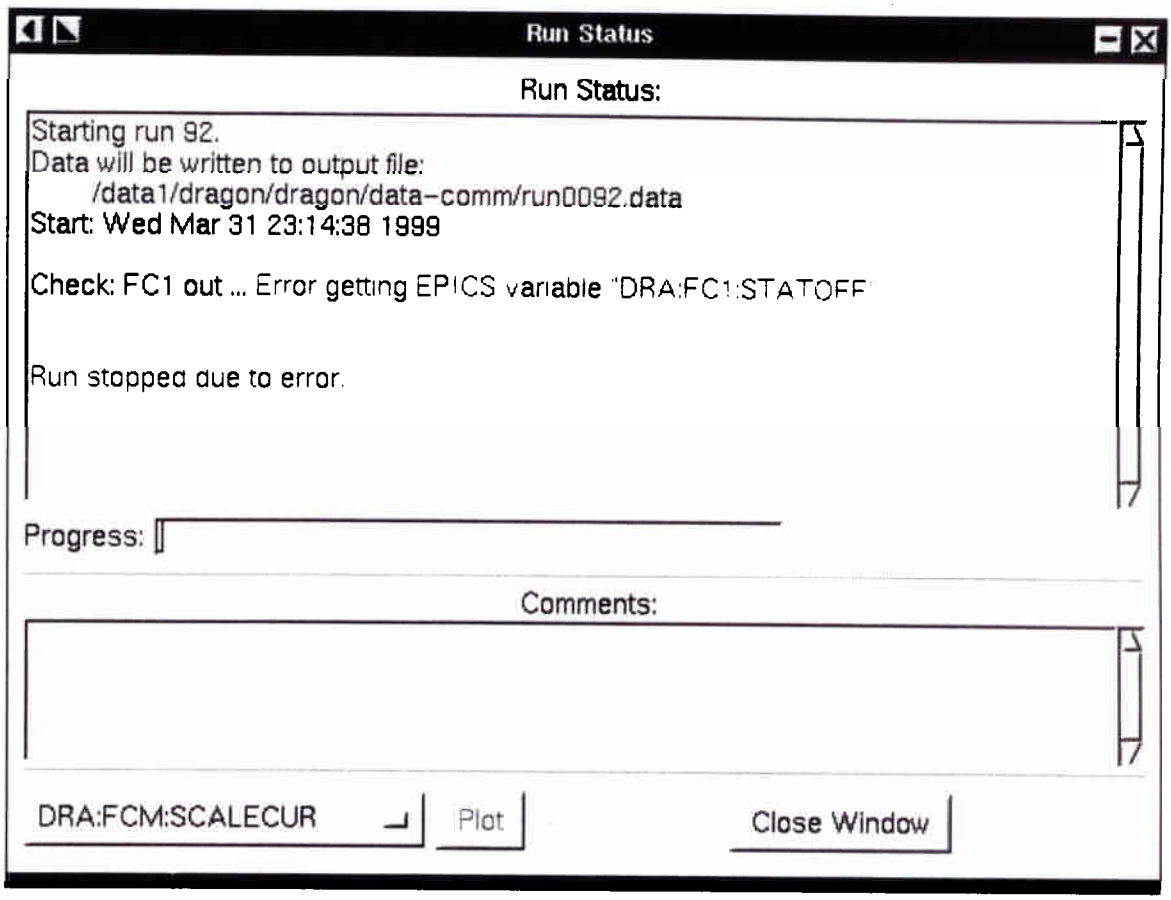

Figure 2: Second **slitscan** window (run status).

When the `Start` button is pushed, the `slitscan` run status window appears (see Figure 2.4). At the beginning of the run, the following actions are performed:

- Check that upstream Faraday cups are out.
- Check that the Faraday cup to be measured is in, that its bias supply is on, and that its gain is set properly.
- Check that upstream slits are not closed.
- Set the slits to their initial positions and widths.
- Begin monitoring setpoints, readbacks, and fields of all electric and magnetic components (the 'watchlist').

After this sequence has been completed, the basic scanning step is to move the slits, wait several seconds, and measure the Faraday cup current. The `slitscan` program allows the currents to be plotted as they are measured by using the `graph` program.[3]

At the end of the run the data file is written in the directory `/data1/dragon/dragon/data-comm/` with a filename containing the run number, such as `run0264.data`. The data file lists the run parameters, the minimum and maximum readings of all 'watchlist' devices, and the beam profile measurements. Monitoring devices on the 'watchlist' provides a full record of DRAGON device settings and allows detection of fault conditions such as tripped power supplies.

2.5 Retuning

At the beginning of this study, the DRAGON tune used during Autumn 2001 was loaded. However, after the first set of scans was completed it was apparent that the focus at the mass and final slits could be improved. Therefore, quadrupole Q1 was adjusted as suggested by Anuj Parikh[4] until a more optimal tune was achieved.[5]

[3] `graph` is part of the GNU `plotutils` package, which is ©Robert Maier and the Free Software Foundation and distributed under the GPL license.

[4] "Alpha Commissioning Studies of DRAGON", Anuj Parikh, 12 Apr 2001.

[5] DRAGON Logbook #6, pg. 39-40, 47.

While the resulting tune was a considerable improvement, the measurements made with the 'old' and 'new' tunes cannot be reasonably compared. Therefore, the retuning effectively doubled the parameter space to be measured. Since the total number of scans was limited by the time allotted, not all parameter combinations were measured.

In particular, measurements at energies of 194 and 200 keV/u are available for the 'old' tune, while energies at 194 and 206 keV/u were measured for the 'new' tune. Clearly, with only two energies measured for each tune it is not possible to distinguish linear and quadratic terms. It was therefore assumed that linear terms dominate the behaviour; quadratic terms were assumed to be zero.

3 Data Analysis

The first step in the data analysis process was to extract the relevant information from the data files and produce a summary file. Subsets of the complete data set were then selected from the summary file in order to isolate parameters. By fitting the centroid positions to a GIOSP-style model, the transfer matrix elements were determined.

The parameters extracted from the data files include the slits measured (charge, mass, or final), the axis (x or y), the wobbler currents (and hence a and b), the tune ('new' or 'old'), and the energy of the run. The centroids and moments of the beam profiles were calculated, and for runs using 'bouncing' the difference between the two half-runs was computed. Since the Faraday cup current measurements have a considerable noise level, zero-clamping was employed; any current values less than 50 pA were set to zero. The 50 pA level was determined empirically to eliminate all measurements consisting of noise while not interfering with the genuine measurements.

In order to convert from wobbler magnet current to beam angles a and b, the approximation employed by Anuj Parikh was used. The wobbler, whose field is dominated by fringe effects, is considered to have an ideal field of some effective length. The current-to-field relationship measured for the wobbler, disregarding hysteresis, was used. From the motion of a charged particle in a magnetic field the angles of ions leaving the wobbler, a and b, can be easily calculated.[6] In this run, typical wobbler currents of ± 50 A gave angles a and b of approximately ± 10 milliradians.

[6] Anuj Parikh, pg. 24.

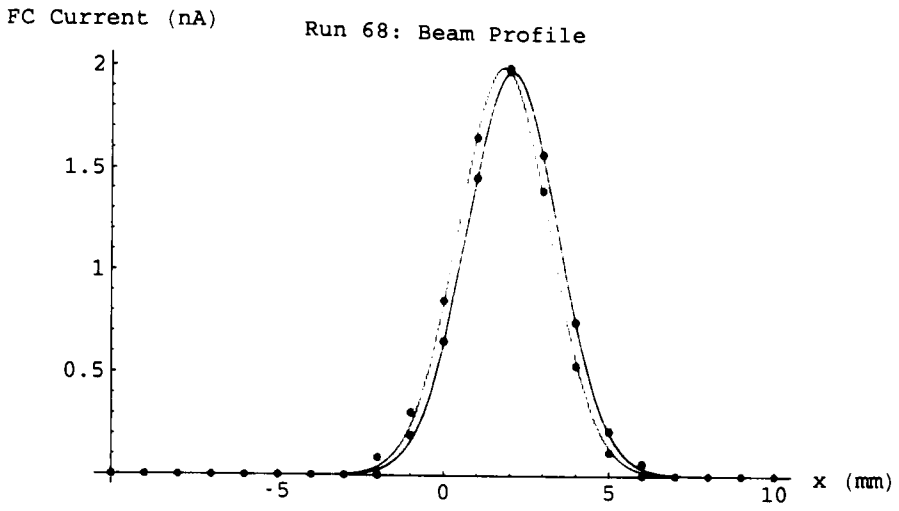

Figure 3: A 'bounced' run in which the halves are considered separately. The fits are Gaussians, with centers 2.07 mm (red) and 1.81 mm (blue).

As discussed earlier, the Faraday cup current measurement circuit employs a (software) low-pass filter with time constant $\tau \simeq 2s$. Thus, if the Faraday cup current changes instantaneously from I_o to I_n at time $t = 0$, the filtered current measured after t seconds will be

$$I_m = I_n + (I_o - I_n)e^{-t/\tau}.$$

Since the slits do not move instantaneously, the measured value is the convolution of the filter impulse response with the Faraday cup current. Extracting the true current from the measured current would require deconvolution, which would require knowledge of the beam profile shape.

Fortunately, the beam profile is continuous and if it is monotonically increasing or decreasing between measurements, the measured value will be closer to the actual value than I_m from above. The **slitscan** program inserted a delay of three to five seconds between measurements. Combined with the movement rate of the slits of approximately one millimeter per second, this ensured that several time constants elapsed, so that the measured value was sufficiently close to the actual value.

The effect of this filtering was apparent in runs employing 'bouncing'. The **slitscan** program's 'Bounce' option makes a beam profile measurement

by first scanning from left to right and then, when the endpoint is reached, 'bouncing back' and scanning right to left. When the scans were split in half and the halves analyzed separately, the calculated centroids were found to be offset by up to 0.4 mm. In Figure 3, for example, the red curve is the profile measured left to right, while the blue curve is measured right to left. The curves are shifted by about 0.26 mm in the direction expected due to the filtering discussed above.

This filtering effect, combined with noise in the Faraday cup measurements and fluctuations in the beam current, limit the accuracy of the centroid values to about ± 0.3 mm. In some of the scans, 'bouncing' was not employed so for these measurements a centroid error estimate of ± 0.5 mm is more accurate.

4 Results

The accuracy of the centroid measurements determines the accuracy to which the GIOSP transfer matrix elements can be determined. In order to find the matrix elements, multiple-parameter fitting was employed. In many cases the best-fit matrix element values were small but non-zero. When a matrix element's contribution to the centroid position was smaller than the noise level of the measurements, it was only possible to bound the absolute value of that element to the level at which its contribution would be measurable.

To find the matrix elements presented below, data sets with a, b, and d values varied were selected. In most of these data sets only three different a and b values and two d values were measured. With these small data sets, statistical analysis was of little use. Therefore, the level at which a best-fit contribution was considered to be a real signal rather than noise was set at $0.5mm$, corresponding to the estimated error in the individual measurements.

The tables presented here list, for each matrix element, the GIOSP simulated value, the measured value or bound, and the contribution to the centroid position that element produces given

$$\sqrt{a^2 + b^2 + (\frac{d}{2})^2} = 0.01$$

which corresponds to a recoil cone angle of 10 milliradians and 2% energy difference. The GIOSP predictions and measured matrix elements are given

in units of metres (x and y), radians (a and b), and fractional energy difference (d).

Where a GIOSP prediction is unavailable, "–" has been given. Where a bound on the measurements has been given, this bound is in the absolute sense: "< 5" means that the matrix element is between -5 and 5. Where an best-fit contribution is below the measurable threshold, "–" has been given.

For a more intuitive presentation of these results, see the next section.

4.1 'Old' Tune

4.1.1 Charge Slits

Element	GIOSP	Measured	Contribution (mm)
$(x_c\|a)$	$-1{\cdot}88 \times 10^{-5}$	$-0{\cdot}18$	$-1{\cdot}8$
$(x_c\|aa)$	$-14{\cdot}9$	-15	$-1{\cdot}5$
$(x_c\|b)$	–	$< 0{\cdot}05$	–
$(x_c\|bb)$	$0{\cdot}49$	< 5	–
$(x_c\|ab)$	–	< 5	–
$(x_c\|d)$	$0{\cdot}30$	$0{\cdot}26$	$5{\cdot}2$
$(x_c\|da)$	$3{\cdot}0$	$< 2{\cdot}5$	–
$(x_c\|db)$	–	$< 2{\cdot}5$	–

Element	GIOSP	Measured	Contribution (mm)
$(y_c\|b)$	$0{\cdot}018$	$0{\cdot}67$	$6{\cdot}7$
$(y_c\|bb)$	–	< 5	–
$(y_c\|a)$	$-0{\cdot}072$	$-0{\cdot}06$	$-0{\cdot}6$
$(y_c\|aa)$	–	< 5	–
$(y_c\|ab)$	$8{\cdot}0$	8	$0{\cdot}4$
$(y_c\|d)$	–	$-0{\cdot}035$	$-0{\cdot}7$
$(y_c\|db)$	–	$< 2{\cdot}5$	–
$(y_c\|da)$	–	$< 2{\cdot}5$	–

4.1.2 Mass Slits

Element	GIOSP	Measured	Contribution (mm)
$(x_m\|a)$	$3{\cdot}9 \times 10^{-6}$	0·31	3·1
$(x_m\|aa)$	0·18	< 5	–
$(x_m\|b)$	–	0·04	0·4
$(x_m\|bb)$	−0·41	< 5	–
$(x_m\|ab)$	–	< 5	–
$(x_m\|d)$	$-8{\cdot}6 \times 10^{-8}$	0·04	0·8
$(x_m\|da)$	−0·43	$< 2{\cdot}5$	–
$(x_m\|db)$	–	$< 2{\cdot}5$	–

Element	GIOSP	Measured	Contribution (mm)
$(y_m\|b)$	−0·43	−0·71	−7·1
$(y_m\|bb)$	–	< 5	–
$(y_m\|a)$	–	−0·24	−2·4
$(y_m\|aa)$	–	< 5	–
$(y_m\|ab)$	6·2	−29	−1·4
$(y_m\|d)$	–	0·056	1·1
$(y_m\|db)$	−4·9	5·7	0·6
$(y_m\|da)$	–	$< 2{\cdot}5$	–

4.1.3 Final Slits

Element	GIOSP	Measured	Contribution (mm)
$(x_f\|a)$	$3{\cdot}9 \times 10^{-7}$	0·66	6·6
$(x_f\|aa)$	$1{\cdot}1 \times 10^{-3}$	5·0	0·5
$(x_f\|b)$	–	−0·03	−0·3
$(x_f\|bb)$	$-7{\cdot}8 \times 10^{-6}$	< 5	–
$(x_f\|ab)$	–	< 5	–
$(x_f\|d)$	$-2{\cdot}7 \times 10^{-7}$	0·08	1·6
$(x_f\|da)$	$-3{\cdot}5 \times 10^{-4}$	−6·3	−0·6
$(x_f\|db)$	–	$< 2{\cdot}5$	–

Element	GIOSP	Measured	Contribution (mm)
$(y_f\|b)$	$-3{\cdot}3 \times 10^{-7}$	0·18	1·8
$(y_f\|bb)$	–	4	0·4
$(y_f\|a)$	–	$< 0{\cdot}05$	–
$(y_f\|aa)$	–	< 5	–
$(y_f\|ab)$	$2{\cdot}8 \times 10^{-5}$	*	*
$(y_f\|d)$	$-2{\cdot}7 \times 10^{-7}$	0·054	1·1
$(y_f\|db)$	$3{\cdot}2 \times 10^{-3}$	5·9	0·6
$(y_f\|da)$	–	$< 2{\cdot}5$	–

Note: $(y_f|ab)$: The measurements with a and b non-zero show large centroid shifts which are not well explained by a linear model. While there is certainly an ab dependence, it is contained in higher-order terms.

4.2 'New' Tune

4.2.1 Charge Slits

Element	GIOSP	Measured	Contribution (mm)
$(x_c\|a)$	$-1{\cdot}88 \times 10^{-5}$	$< 0{\cdot}05$	–
$(x_c\|aa)$	−14·9	−16	−1·6
$(x_c\|b)$	–	$< 0{\cdot}05$	–
$(x_c\|bb)$	0·49	< 5	–
$(x_c\|ab)$	–	< 5	–
$(x_c\|d)$	0·30	0·25	5·1
$(x_c\|da)$	3·0	2·4	0·2
$(x_c\|db)$	–	$< 2{\cdot}5$	–

Element	GIOSP	Measured	Contribution (mm)
$(y_c\|b)$	0·018	−0·14	−1·4
$(y_c\|bb)$	–	< 5	–
$(y_c\|a)$	−0·072	$< 0{\cdot}05$	–
$(y_c\|aa)$	–	< 5	–
$(y_c\|ab)$	8·0	5	0·5
$(y_c\|d)$	–	0·036	0·7
$(y_c\|db)$	–	3·1	0·3
$(y_c\|da)$	–	$< 2{\cdot}5$	–

4.2.2 Mass Slits

Element	GIOSP	Measured	Contribution (mm)
$(x_m\|a)$	$3{\cdot}9 \times 10^{-6}$	0·025	0·5
$(x_m\|aa)$	0·18	< 5	–
$(x_m\|b)$	–	$< 0{\cdot}05$	–
$(x_m\|bb)$	−0·41	< 5	–
$(x_m\|ab)$	–	< 5	–
$(x_m\|d)$	$-8{\cdot}6 \times 10^{-8}$	$< 0{\cdot}025$	–
$(x_m\|da)$	−0·43	$< 2{\cdot}5$	–
$(x_m\|db)$	–	$< 2{\cdot}5$	–

Element	GIOSP	Measured	Contribution (mm)
$(y_m\|b)$	−0·43	−0·29	−2·9
$(y_m\|bb)$	–	< 5	–
$(y_m\|a)$	–	−0·36	−3·6
$(y_m\|aa)$	–	< 5	–
$(y_m\|ab)$	6·2	5	0·3
$(y_m\|d)$	–	0·07	1·4
$(y_m\|db)$	−4·9	−6·0	−0·6
$(y_m\|da)$	–	$< 2{\cdot}5$	–

4.2.3 Final Slits

Element	GIOSP	Measured	Contribution (mm)
$(x_f\|a)$	$3{\cdot}9 \times 10^{-7}$	0·45	4·5
$(x_f\|aa)$	$1{\cdot}1 \times 10^{-3}$	< 5	–
$(x_f\|b)$	–	$< 0{\cdot}05$	–
$(x_f\|bb)$	$-7{\cdot}8 \times 10^{-6}$	< 5	–
$(x_f\|ab)$	–	< 5	–
$(x_f\|d)$	$-2{\cdot}7 \times 10^{-7}$	$< 0{\cdot}025$	–
$(x_f\|da)$	$-3{\cdot}5 \times 10^{-4}$	−8·4	−0·8
$(x_f\|db)$	–	$< 2{\cdot}5$	–

Element	GIOSP	Measured	Contribution (mm)
$(y_f\|b)$	$-3{\cdot}3 \times 10^{-7}$	$-0{\cdot}10$	$-1{\cdot}0$
$(y_f\|bb)$	–	< 5	–
$(y_f\|a)$	–	$< 0{\cdot}05$	–
$(y_f\|aa)$	–	5	$0{\cdot}5$
$(y_f\|ab)$	$2{\cdot}8 \times 10^{-5}$	< 5	–
$(y_f\|d)$	$-2{\cdot}7 \times 10^{-7}$	$0{\cdot}061$	$1{\cdot}2$
$(y_f\|db)$	$3{\cdot}2 \times 10^{-3}$	4	$0{\cdot}4$
$(y_f\|da)$	–	$< 2{\cdot}5$	–

4.3 Plots

This study measured the elements of the matrix that transforms an ion's initial a, b, and d values into its x and y positions at the charge, mass, and final slits. In the plots below, we consider initial parameters that lie on the surface of the ellipsoid

$$\sqrt{a^2 + b^2 + (\frac{d}{2})^2} = 0.01.$$

We take slices of this ellipsoid in planes of constant d and follow these circles (in the a-b plane) through the transfer matrix. Since the a-x and b-y values are more strongly linked than are the cross-terms, these circles tend to be transformed into stretched loops in (x,y) space. In order the allow the stretching to be visualized, points uniformly distributed around the circle in (a,b) space are plotted in (x,y) space.

In order to separate the different curves, a colour scheme has been used. The red curve corresponds to a positive d value, the middle green curve has $d = 0$, and the purple curve shows a negative d. Considering the d direction to be the vertical in the a-b-d ellipsoid, the curves show slices with polar angles in multiples of $\pi/8$ from one (red) to seven (purple).

The points plotted on the curves, similarly, are azimuthal angles in the (a,b) plane in multiples of $\pi/4$. The points corresponding to maximum positive a and b are labelled.

The plots are given in groups of three, showing the 'old' tune, 'new' tune, and GIOSP predictions. The scales of these groups are the same and the aspect ratio has been fixed at one to allow intuitive interpretation of the shape of the beam profiles.

The GIOSP prediction for the final slits has not been shown because the profile is completely contained in a square micrometer so is barely visible at the scale shown here.

Two points about the beam profiles should be kept in mind. First, these plots show the positions of the *centroids* of the beam; the actual beam density distributions will be broader. Second, in normal operation the a, b, and d parameters cannot be controlled (since they result from the recoil kinematics) so the beam spot size will be the outline of the coloured curves shown here, expanded by the beam width.

It is interesting to note that for both the measured and GIOSP predicted profiles at the charge slits, the beam is spatially dispersed according to energy. At the final slits for the 'new' tune this effect is apparent to a lesser extent. Presumably, a position- and energy-sensitive detector such as a silicon strip detector could be used to measure this correlation.

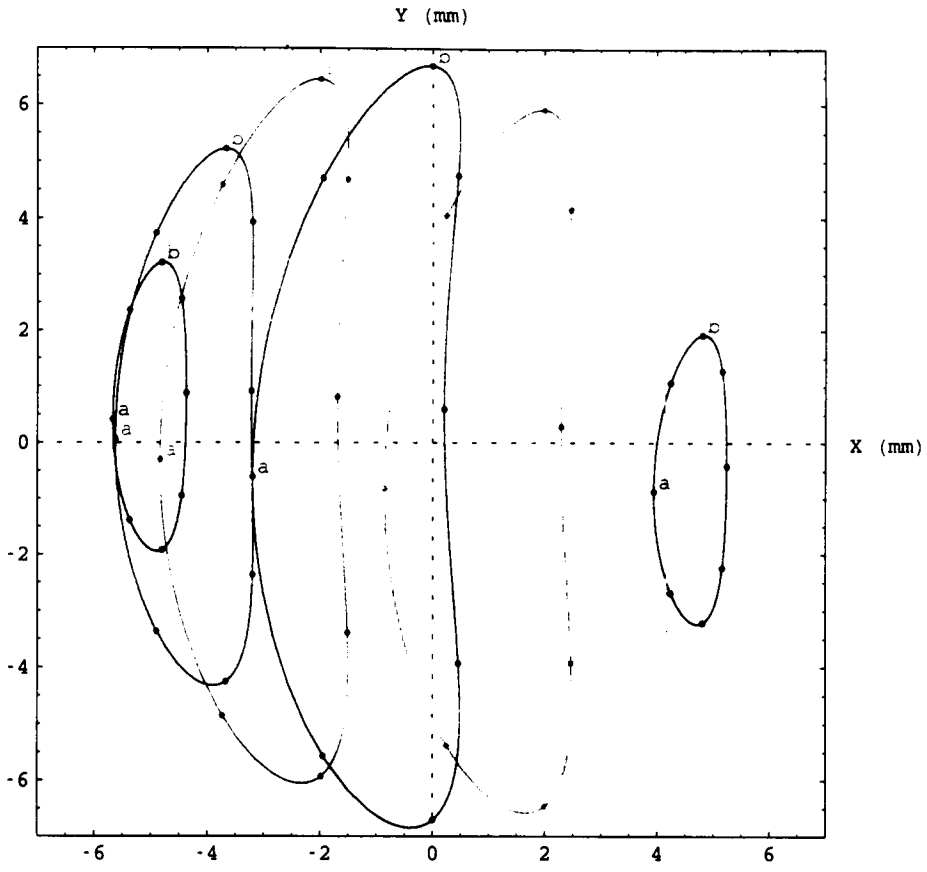

Figure 4: Charge Slits: Measurement (Old Tune)

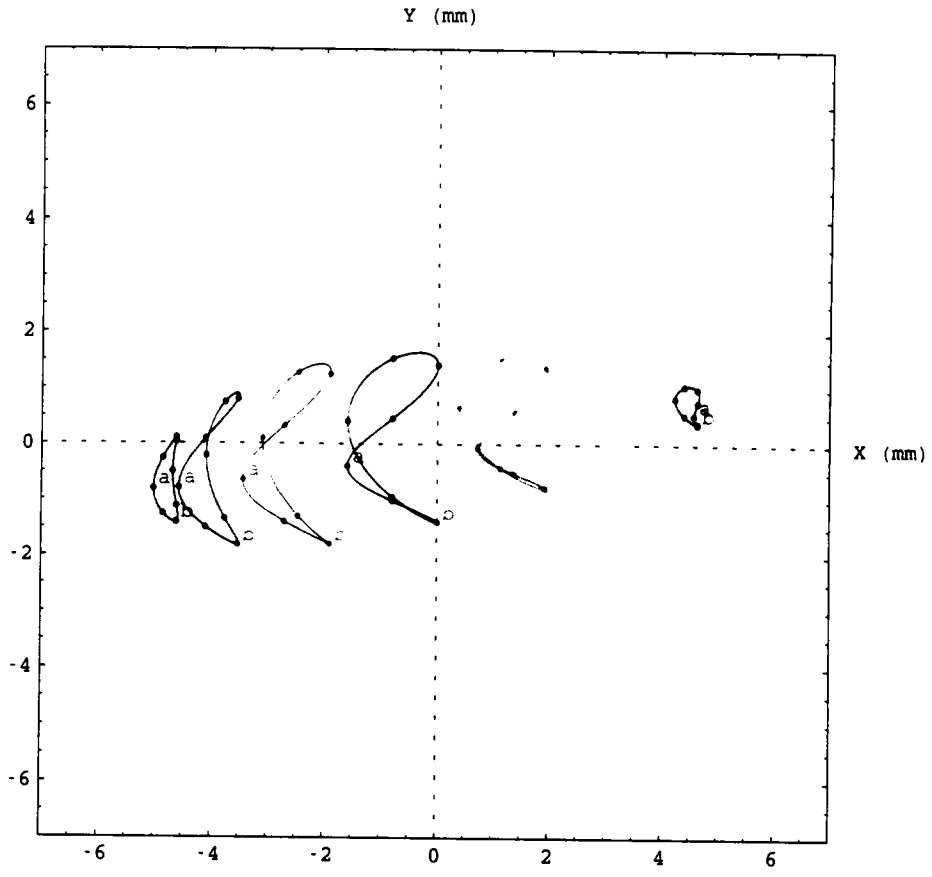

Figure 5: Charge Slits: Measurement (New Tune)

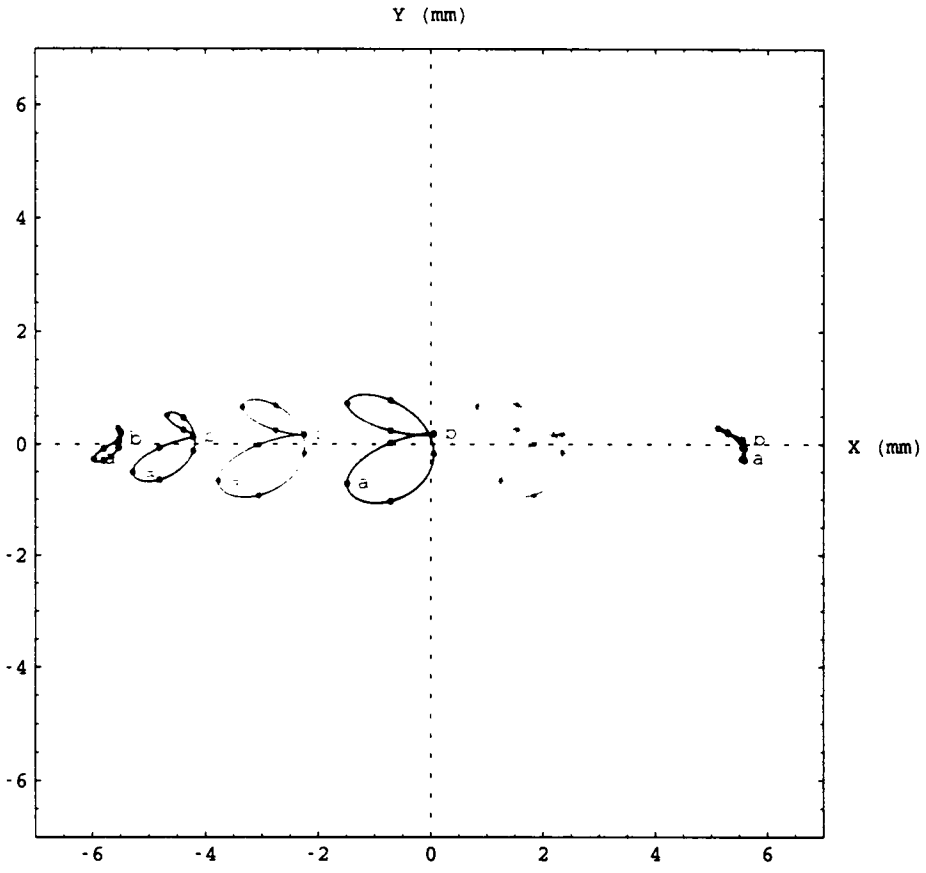

Figure 6: Charge Slits: Simulation

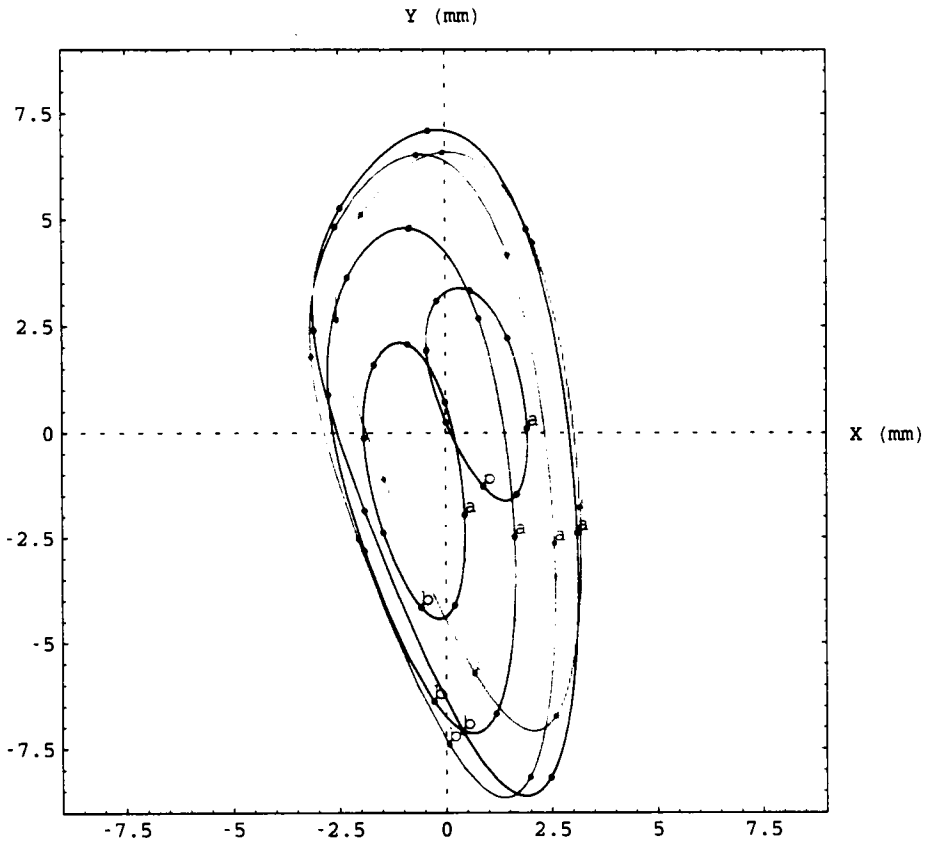

Figure 7: Mass Slits: Measurement (Old Tune)

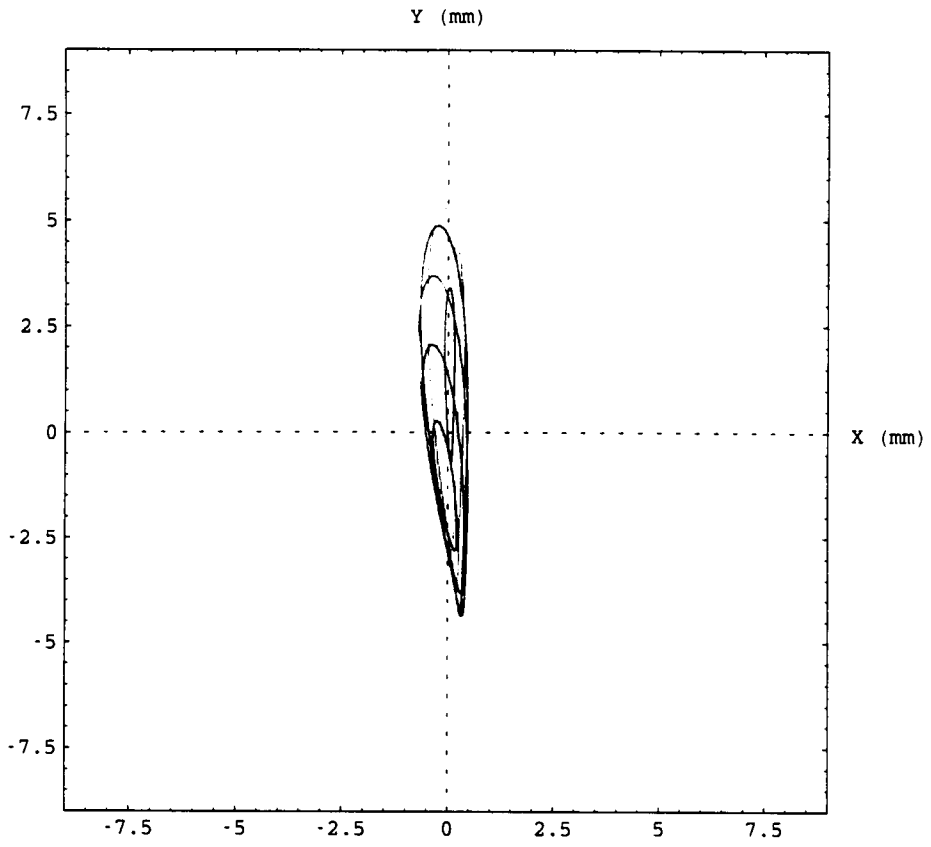

Figure 8: Mass Slits: Measurement (New Tune)

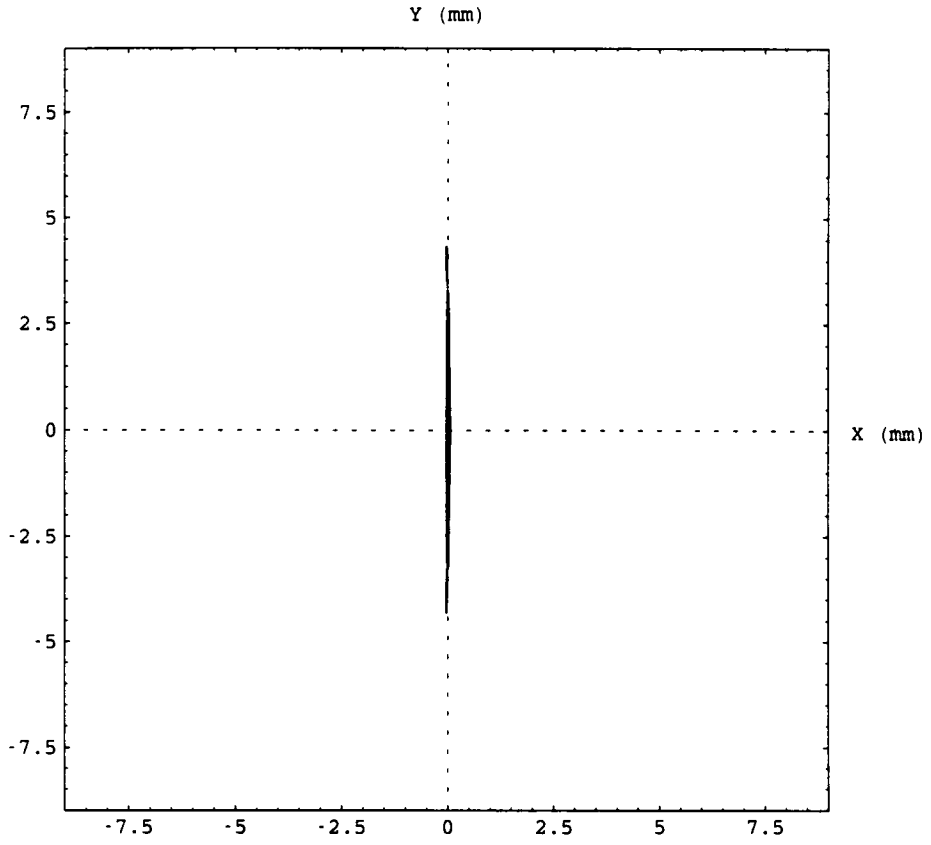

Figure 9: Mass Slits: Simulation

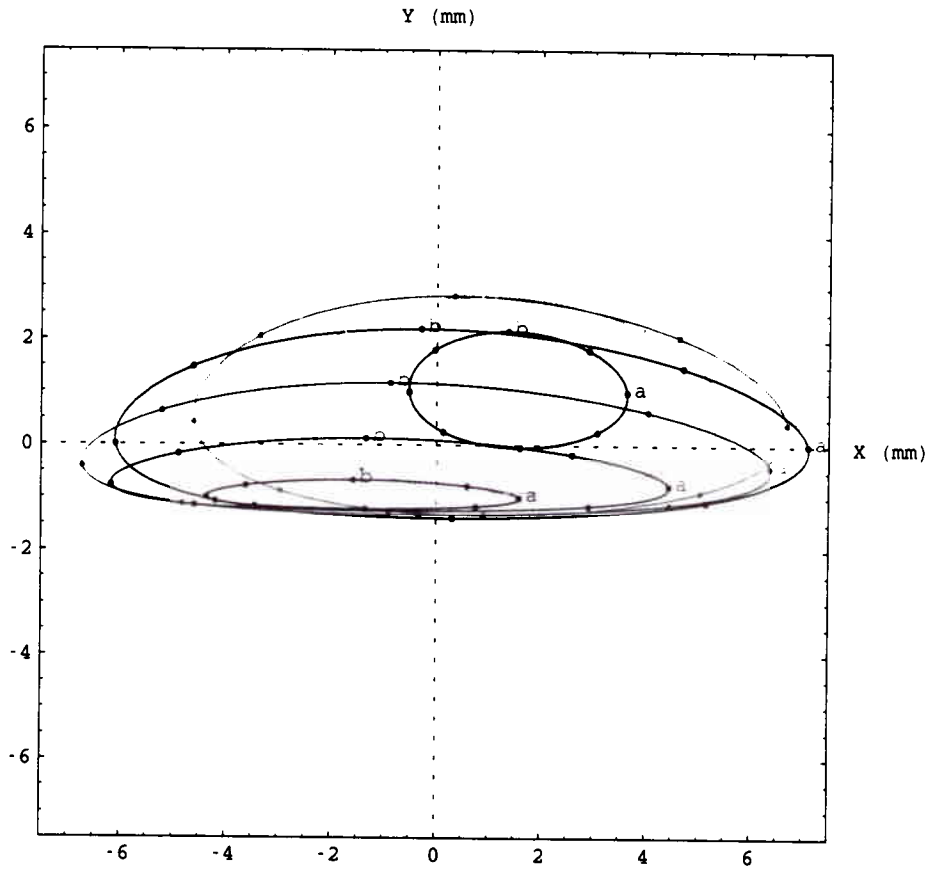

Figure 10: Final Slits: Measurement (Old Tune)

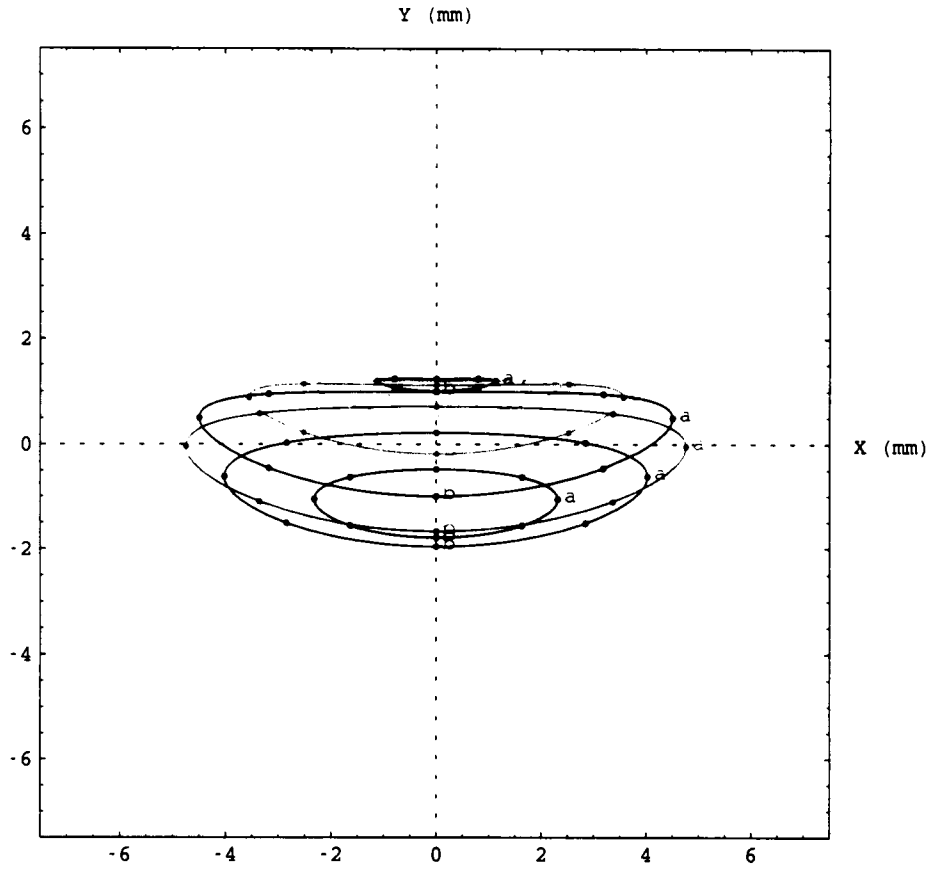

Figure 11: Final Slits: Measurement (New Tune)

5 Conclusions

Although the matrix elements measured differ significantly from the GIOSP predictions, they nevertheless show that for typical recoil cone angles the beam envelopes at the charge, mass, and final slits are reasonably sized. From the plots it is clear that the 'new' tune shows a considerably better focus.

This study has shown that slits and Faraday cups can be effectively used to measure beam profiles. The major obstacle in this process was the software filtering of the Faraday cup currents, which forced the `slitscan` software to insert several second waits before each current measurement. As a result, the number of scans that could be performed was lower than expected and the data set was therefore somewhat sparse. This effect was exacerbated by the retuning midway through the study. However, enough measurements were available to determine the most important first-order matrix terms and most of the second-order ones.